Received 5 November 2024; revised 26 December 2024; accepted 5 January 2025. Date of publication 13 January 2025; date of current version 26 March 2025.

*Digital Object Identifier 10.1109/OJAP.2025.3528232*

# Synthesis of Wide-Angle Scanning Arrays Through Array Power Control

**PIETRO ROSATTI[1,2] (Student Member, IEEE), GIACOMO OLIVERI[1,2] (Fellow, IEEE), AND ANDREA MASSA[1,2,3,4,5] (Fellow, IEEE)**

[1]Department of Civil, Environmental, and Mechanical Engineering, ELEDIA Research Center, University of Trento, 38123 Trento, Italy
[2]ELEDIA Research Unit, CNIT - University of Trento, 38123 Trento, Italy
[3]School of Electronic Engineering, ELEDIA Research Center, UESTC, Chengdu 611731, China
[4]ELEDIA Research Center, Tsinghua University, Beijing 100084, China
[5]School of Electrical Engineering, Tel Aviv University, Tel Aviv 69978, Israel

CORRESPONDING AUTHOR: A. MASSA (e-mail: andrea.massa@unitn.it)

This work was supported in part by the Project DICAM-EXC (Departments of Excellence 2023–2027), funded by the Italian Ministry of Education, Universities and Research (MUR) under Grant L232/2016; in part by the Project “Smart ElectroMagnetic Environment in TrentiNo - SEME@TN” funded by the Autonomous Province of Trento under Grant CUP: C63C22000720003; in part by the Project “AURORA - Smart Materials for Ubiquitous Energy Harvesting, Storage, and Delivery in Next Generation Sustainable Environments” funded by the Italian Ministry for Universities and Research within the PRIN-PNRR 2022 Program; and in part by Projects funded by the European Union - NextGenerationEU within the PNRR Program through the Project “ICSC National Centre for HPC, Big Data and Quantum Computing (CN HPC)” under Grant CUP: E63C22000970007, through the Project “Telecommunications of the Future (PE00000001 - Program “RESTART,” Structural Project 6GWINET) under Grant CUP: D43C22003080001, through the Project INSIDE-NEXT - Indoor Smart Illuminator for Device Energization and Next-Generation Communications under Grant CUP: E53D23000990001, and through the Project “Telecommunications of the Future (PE00000001 - Program RESTART, Focused Project MOSS) under Grant CUP: J33C22002880001.

**ABSTRACT** A new methodology for the synthesis of wide-angle scanning arrays is proposed. It is based on the formulation of the array design problem as a multi-objective one where, for each scan angle, both the radiated power density in the scan direction and the total reflected power are accounted for. A set of numerical results from full-wave simulated examples - dealing with different radiators, arrangements, frequencies, and number of elements - is reported to show the features of the proposed approach as well as to assess its potentialities. A widening of the field-of-view percentage of up to 22% with respect to standard scanning methods is demonstrated.

**INDEX TERMS** Wide-angle scanning, excitation design, array synthesis, active reflection coefficient stabilization, multi-objective evolutionary optimization.

## I. INTRODUCTION AND MOTIVATION

Wide-angle scanning is one of the key requirements in modern antenna arrays for communications and sensing [1], [2]. Indeed, stable radiation performance over a wide range of steering angles are increasingly important in several applicative scenarios such as wireless coverage, automotive radars, satellite communications, and imagers [1], [2], [3]. Unfortunately, the gain/directivity of antenna arrays typically worsens as the scan angle increases, specifically in the presence of “blind spots” [1], [2], and it limits the array field-of-view (*FoV*) [1], [2]. These undesired phenomena are a direct consequence of the instability of the active return loss (*ARL*) versus the scan angle [4]. In the last decades, several approaches have been introduced in the state-of-the-art (*SoA*) literature to improve the *ARL* stability and to increase the *FoV* of phased arrays by mitigating the inter-element coupling [3], [5], [6], [7], [8], [9], [10], [11], [12], [13]. More in detail, the exploitation of ad-hoc solutions such as the use of cavities [5], [6] or magnetic dipoles [7] has been proposed to individually insulate the array elements. An alternative strategy, not involving complex radiators, resorts to the introduction of decoupling feed networks [8], [9], [14], which synthesis and implementation become very challenging when a wideband working is required [8], [9], [14]. Wide-angle impedance matching (*WAIM*) layers coating the array and based either on standard [15] or artificial materials [3], [10], [11], [12], [13] has been also adopted to stabilize the *ARL*. Nonetheless, this latter solution - as well as the previous ones - needs non-trivial updates of the system hardware, as applied to existing architectures, and customized designs/implementations strongly depend on the adopted antenna technology [3], [10], [11], [12], [13].

Otherwise, the *ARL* stabilization may be yielded without architectural modifications by considering a completely different perspective, as well. In fact, the *ARL* depends not only on the inter-element coupling, but also on the excitations applied to each elementary radiator of the array [4], [16]. While the synthesis of such excitations is typically aimed at controlling the scan direction, the sidelobe profile [17], and/or more advanced quality-of-service indicators [18], [19], there are not theoretical obstacles to even address the stabilization the *ARL* still fulfilling the user-desired pattern features when scanning.

Following this line of reasoning, an innovative methodology for the synthesis of wide-scanning arrays is proposed into the following. Such an approach is based on the formulation of the array synthesis as a multi-objective problem where, for each scan angle, both the radiated power density in the scan direction and the total reflected power are accounted for by including the finite array coupling in the design process (i.e., no periodicity approximation is employed).

Accordingly, the main innovative contributions of this work include (*i*) for the first time to the best of the authors' knowledge, the synthesis of the array excitations to minimize the reflected power, while keeping suitable radiation performance, for widening the *FoV* in finite arrays, (*ii*) the full-wave numerical proof for both linear and planar arrays that it is possible to obtain wider scan angles without modifying the antenna architecture, hence implicitly the assessment of the applicability of the proposed concept to upgrade existing arrays, and (*iii*) the derivation of a general-purpose strategy for wide angle scanning that, unlike *SoA* methods [3], [5], [6], [7], [8], [9], [10], [11], [12], [13], can be adopted regardless of the underlying antenna technology and/or physical implementation details.

The outline of the paper is as follows. The mathematical formulation of the array synthesis problem at hand is formulated in Section II, where the proposed excitation-based approach to yield wide-angle scanning performance is presented, as well. A set of numerical results from full-wave simulated examples is reported to show the features of the proposed strategy as well as to assess its potentialities in different working conditions and also in comparison with state-of-the-art competitive techniques (Section III). Finally, some conclusions are drawn (Section IV).

## II. MATHEMATICAL FORMULATION

Consider the scenario in Fig. 1 where an antenna array of $N$ elements, each one described by the $L$ geometrical parameters $\underline{g} = \{g_l;\, l = 1, \ldots, L\}$ and operating at the carrier frequency $f_0$, is fed by the set of $N$ incident excitation coefficients $\underline{w}_q^+ \triangleq \left\{w_{nq}^+;\, n = 1, \ldots, N\right\}$ to radiate a beampattern steered at the $q$-th ($q = 1, \ldots, Q$) scan angle $\left(\theta_q, \varphi_q\right)$ [4], [16], [20]. The corresponding reflected

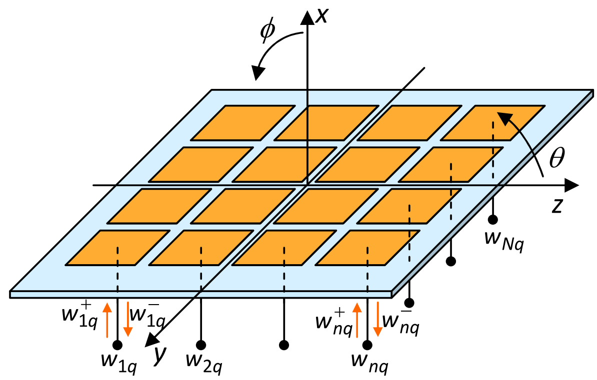


**FIGURE 1.** ***Problem geometry.*** **Sketch of the reference phased array layout.**

excitation coefficients, measured at the $n$-th ($n = 1, \ldots, N$) element, of the array are defined as [16]

$$w_{nq}^- \triangleq w_{nq}^+ \times \Gamma_{nq} \tag{1}$$

where

$$\Gamma_{nq} \triangleq \sum_{m=1}^{N} S_{nm} \frac{w_{mq}^+}{w_{nq}^+} \tag{2}$$

it the $n$-th ($n = 1, \ldots, N$) element active reflection coefficient at the $q$-th ($q = 1, \ldots, Q$) scan angle, the corresponding *ARL* being $ARL_{nq} \triangleq \left|\Gamma_{nq}\right|^2$ ($n = 1, \ldots, N$; $q = 1, \ldots, Q$) [3], [4], [10], [11], [12], [13], and $S_{nm}$ is the ($n$, $m$)-th ($n$, $m = 1, \ldots, N$) entry of the $N \times N$ scattering matrix $\mathcal{S}$ [4], [16], [17], [20]. This latter univocally models the array inter-element coupling effects that, unlike $\Gamma_{nq}$ (2) and $w_{nq}^-$ (1), does not depend on the applied array excitations $w_{nq}^+$.

Under the above assumptions, the total excitation at the $n$-th ($n = 1, \ldots, N$) array element, $w_{nq}$ ($w_{nq} \triangleq w_{nq}^+ + w_{nq}^-$) turns out to be [16], [20]

$$w_{nq} = \left(1 + \Gamma_{nq}\right) w_{nq}^+, \tag{3}$$

then field radiated by the $N$-elements antenna array in the Fraunhofer region has the following expression [16], [17], [20]

$$\mathbf{E}\left(.\mathbf{r}|\underline{w}_q\right) = \frac{jk_0}{2\pi} \frac{\exp(-jk_0 r)}{r} \sum_{n=1}^{N} w_{nq} \exp\left[-jk_0(\mathbf{r}_n \cdot \widehat{\mathbf{r}})\right] \mathbf{E}_n(\theta, \varphi), \tag{4}$$

which holds true regardless of the array geometry (linear/planar) and element polarization (i.e., single/dual polarization). In (4), $k_0$ is the free-space wavenumber, $\mathbf{r} = \{r, \theta, \varphi\}$ is the spatial coordinate ($\widehat{\mathbf{r}} = \frac{\mathbf{r}}{|\mathbf{r}|}$), $\cdot$ stands for the scalar product, and $\mathbf{r}_n$ is the location of the $n$-th ($n = 1, \ldots, N$) array element, which element pattern is $\mathbf{E}_n(\theta, \varphi)$ [17]. It is worth pointing out that in finite arrays, the element pattern is different for each $n$-th ($n = 1, \ldots, N$) element [i.e., $\mathbf{E}_n(\theta, \varphi) \neq \mathbf{E}_m(\theta, \varphi)$, $n \neq m$ ($n$, $m$ =

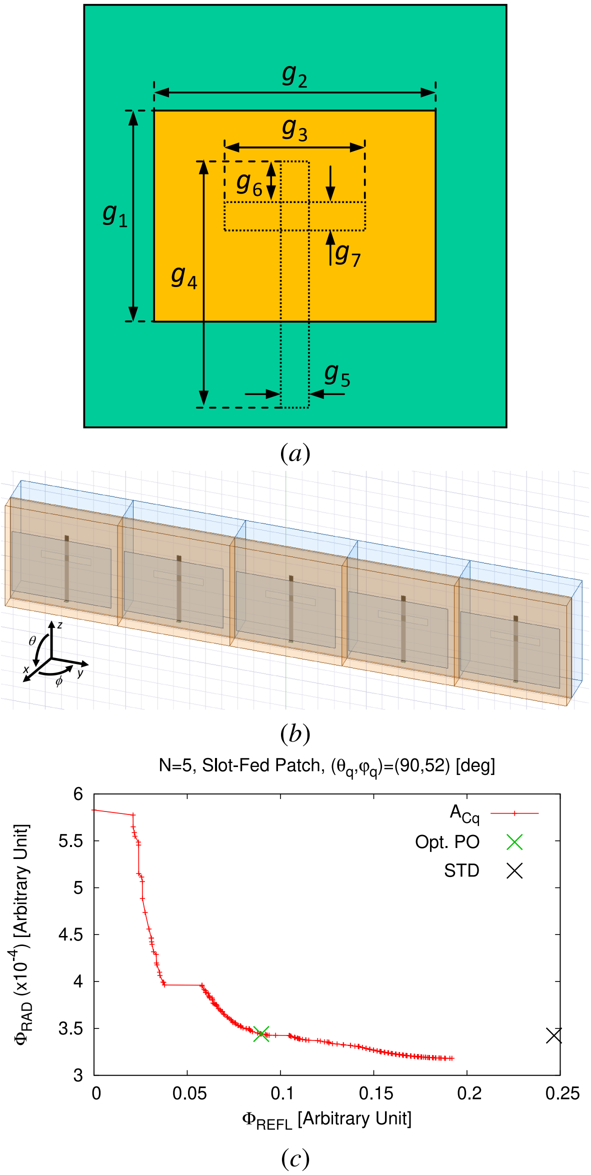


**FIGURE 2.** ***Slot-fed patch linear array*** **($N = 5$, $f = 2$ [GHz], $d = 0.47\lambda$) - Sketch of (a) the geometry of array element and (*b*) the HFSS model of the array, and plot of the Pareto-optimal solutions when $(\theta_q, \varphi_q) = (90, 52)$ [deg].**

$1, \dots, N)$], even though the centrally-located radiators of large arrays exhibit very similar angular responses [17].

The power density radiated along the direction $(\theta, \varphi)$ by the array steered towards $(\theta_q, \varphi_q)$ is obtained from (4) as follows

$$\psi_q(\theta, \varphi) = \lim_{r\to\infty} \frac{r^2}{2\nu}\left|\mathbf{E}\left(\mathbf{r}|\underline{w}_q\right)\right|^2 \tag{5}$$

and the total radiated power is $\mathbb{P}_q^{RAD} = \int_\Omega \psi_q(\theta, \varphi) d\Omega$, $\Omega$ being a far-field closed surface surrounding the array. Moreover, the total reflected power percentage is defined as

$$\zeta_q = \frac{\mathbb{P}_q^{REFL}}{\mathbb{P}_q^{IN}} \tag{6}$$

where $\mathbb{P}_q^{IN}$ and $\mathbb{P}_q^{REFL}$ are the input power ($\mathbb{P}_q^{IN} \triangleq \sum_{n=1}^{N}\left|w_{nq}^{+}\right|^2$) and the reflected power ($\mathbb{P}_q^{REFL} \triangleq \sum_{n=1}^{N}\left|w_{nq}^{-}\right|^2$ equal to $\mathbb{P}_q^{REFL} \triangleq \sum_{n=1}^{N} ARL_{nq}\left|w_{nq}^{+}\right|^2$) when the array is steered along $\left(\theta_q, \varphi_q\right)$, respectively. According to these definitions, the *FoV* of an antenna array can be identified as the angular range $\Omega_{FoV}$ ($\Omega_{FoV} \subset \Omega_{TOT}$, $\Omega_{TOT} = \left\{\left(\theta_q, \varphi_q\right);\ q = 1, \dots, Q\right\}$) where the radiated power density in the scan direction $\left(\theta_q, \varphi_q\right)$ is greater than a threshold $\psi_{TH}$ (i.e., $\psi_q\left(\theta_q, \varphi_q\right) \geq \psi_{TH}$) and the total reflected power percentage is smaller than a target value $\zeta_{TH}$ (i.e., $\zeta_q \leq \zeta_{TH}$). Mathematically, it turns out that $\left(\theta_q, \varphi_q\right) \in \Omega_{FoV}$ if

$$\begin{aligned}\psi_q\left(\theta_q, \varphi_q\right) &\geq \psi_{TH}\\ \zeta_q &\leq \zeta_{TH}.\end{aligned} \tag{7}$$

In order to achieve wide scan performance (i.e., a wide *FoV*), *SoA* methods in the reference literature [3], [5], [6], [7], [8], [9], [10], [11], [12], [13] require an $ARL_{nq}$ almost independent on the angular direction (i.e., $ARL_{nq} \approx ARL_n$) and smaller than an application-defined threshold $ARL_{TH}$ ($ARL_n \leq ARL_{TH}$) by enforcing the condition $|S_{nm}| \to 0$ ($n = 1, \dots, N$; $m = 1, \dots, M$; $m \neq n$) to yield

$$\Gamma_n\left(\theta_q, \varphi_q\right) \approx S_{nn}. \tag{8}$$

Therefore, the condition $ARL_n \leq ARL_{TH}$ is fulfilled by properly setting the descriptors of the elementary radiator, $\underline{g}$, so that $|S_{nn}|^2 \leq ARL_{TH}$, while the incident excitation coefficients $\underline{w}_q^{+}$ are optimized to fulfill the requirements on the radiated power density along $\left(\theta_q, \varphi_q\right)$, $\psi_q\left(\theta_q, \varphi_q\right)$.

Otherwise, the proposed approach leverages the observation that, according to (2), for a given matrix $\mathcal{S}$ (i.e., resulting from the definition of the element geometries, physical properties, and positions), both the total reflected power percentage, $\zeta_q$, and the radiation properties of the array $\mathbf{E}\left(\mathbf{r}|\underline{w}_q\right)$ (4) can be controlled by properly optimizing the excitations $\underline{w}_q^{+}$ ($q = 1, \dots, Q$) to maximize the *FoV* of the antenna array. Therefore, the design of the optimal excitations for the $q$-th ($q = 1, \dots, Q$) scan angle, $\left.\underline{w}_q^{+}\right\rfloor_{opt}$, is mathematically formulated as a multi-objective constrained optimization where $\left.\underline{w}_q^{+}\right\rfloor_{opt}$ is the set of excitations $\underline{w}_q^{+}$ that fulfils some feasibility conditions (i.e., $\underline{w}^{+} \in \mathcal{W}$, $\mathcal{W}$ being a set of requirements on the excitation coefficients such as constant magnitude, phase quantization, etc$\cdots$), while minimizing the $T = 2$ objective functions coding the *FoV* condition (7)

$$\left.\underline{w}_q^{+}\right\rfloor_{opt} \triangleq \arg\left\{\min_{\underline{w}_q^{+}}\left[\Phi_{REFL}\left(\underline{w}_q^{+}\right);\ \Phi_{RAD}\left(\underline{w}_q^{+}\right)\right]\right\}. \tag{9}$$

In (9), the first objective function $\Phi_{REFL}$ coincides with the total reflected power percentage when the array is steered along $\left(\theta_q, \varphi_q\right)$

$$\Phi_{REFL}\left(\underline{w}_q^{+}\right) \triangleq \zeta_q, \tag{10}$$

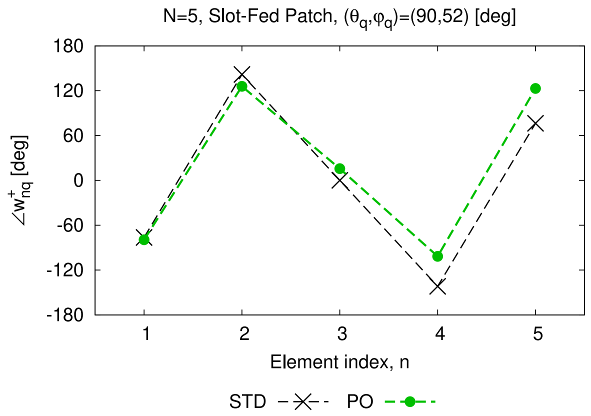


$(a)$

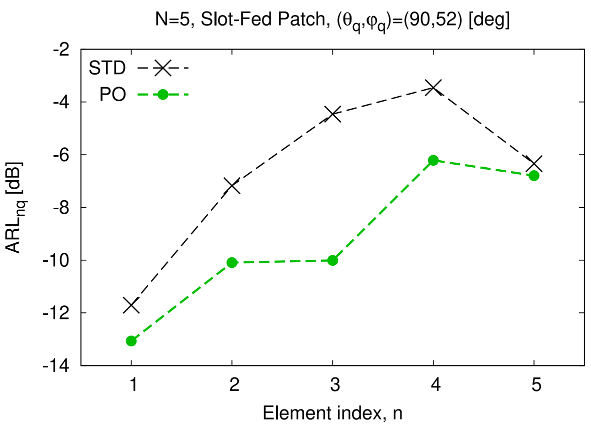


$(b)$

**FIGURE 3.** ***Slot-fed patch linear array*** **($N = 5$, $f = 2$ [GHz], $d = 0.47\lambda$, $q = 53$, $(\theta_q, \varphi_q) = (90, 52)$ [deg]) - Plots of (a) $\angle w^+_{nq}$ and ($b$) $ARL_{nq}$, $n = 1, \ldots, N$.**

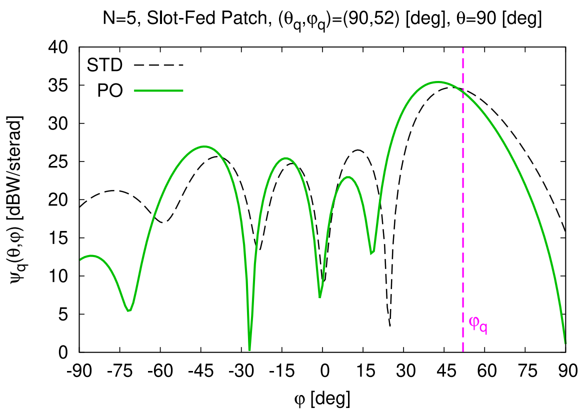


**FIGURE 4.** ***Slot-fed patch linear array*** **($N = 5$, $f = 2$ [GHz], $d = 0.47\lambda$, $q = 53$, $(\theta_q, \varphi_q) = (90, 52)$ [deg], $\theta = 90$ [deg]) - Plot of $\psi_q(\theta, \varphi)$.**

while the second one, $\Phi_{RAD}$, is defined as the inverse of the power density radiated along the $q$-th ($q = 1, \ldots, Q$) steering direction

$$\Phi_{RAD}\left(\underline{w}^+_q\right) = \frac{1}{\psi_q\left(\theta_q, \varphi_q\right)}. \tag{11}$$

The synthesis process at hand does not involve the geometrical descriptors of the array, $\underline{g}$, which are user-defined and *a-priori* set.

Since (9) codes a multi-objective optimization problem, which involves highly non-linear cost function terms, and the unknowns (i.e., magnitude/phase of the $\underline{w}^+$ entries) are real-valued, a multi-objective steady-state evolutionary algorithm that uses $\varepsilon$-dominance archiving ($\varepsilon$-*MOEA*) to record a diverse set of Pareto optimal solutions has been adopted [22], [23], [24].

Unlike generational algorithms [25], the $\varepsilon$-*MOEA* evolves one solution at a time to ensure convergence and diversity throughout the optimization process [22], [23], [24]. For each $q$-th ($q = 1, \ldots, Q$) scan angle, $\left(\theta_q, \varphi_q\right)$, the following iterative procedure ($c$ being the iteration index) is performed. At each $c$-th ($c = 1, \ldots, C$) iteration, both a variable-sized Pareto front $\mathcal{A}_{cq}$ of $A_{cq}$ solutions $[\mathcal{A}_{cq} = \left\{\left.\underline{w}^+_q\right]^{(a)}_c;\ a = 1, \ldots, A_{cq}\right\}]$ and a fixed size population $\mathcal{P}_{cq}$ of $P$ individuals $[\mathcal{P}_{cq} = \left\{\left.\underline{w}^+_q\right]^{(p)}_c;\ p = 1, \ldots, P\right\}]$ are evolved according to the $\varepsilon$-*MOEA* mutation, recombination, and selection operators with control parameters $\underline{\varepsilon} = \{\varepsilon_1, \varepsilon_2\}$ [22], [23], [24]. At the convergence (i.e., $c = C$), a Pareto front of non-dominated excitation sets $\mathcal{A}_{Cq}$ is outputted and the user identifies the optimal one according to a criterion based on either functional (i.e., a set of conditions on $\Phi_{RAD}$ and/or $\Phi_{REFL}$) or non-functional (e.g., costs, maintenance, etc$\cdots$ ) constraints. Finally, the *FoV* $\Omega_{FoV}$ of the synthesized array (i.e., $\left.\underline{\underline{W}}^+\right]_{opt} = \left\{\left.\underline{w}^+_q\right]_{opt};\ q = 1, \ldots, Q_{FoV}\right\}$) turns out to be the set of $Q_{FoV}$ ($Q_{FoV} \leq Q$) adjacent scan directions for which (7) holds true.

## III. NUMERICAL RESULTS

This section is aimed at both illustrating the features of the proposed method and assessing its effectiveness also in comparison with state-of-the-art solutions.

The first numerical example deals with a linear array of $N = 5$ equally-spaced by $d = 0.47\lambda$ cavity-backed slot-fed microstrip antennas [Fig. 2($a$)] printed on a Polyflon CuFlon substrate with thickness $9 \times 10^{-3}$ [m]. Each radiator [Fig. 2($b$)] has been modeled in Ansys HFSS [27] by choosing the following $L = 7$ descriptors to operate at $f = 2$ GHz: $g_1 = 4.13 \times 10^{-2}$ [m], $g_2 = 6.18 \times 10^{-2}$ [m], $g_3 = 3.09 \times 10^{-2}$ [m], $g_4 = 4.58 \times 10^{-2}$ [m], $g_5 = 2.54 \times 10^{-3}$ [m], $g_6 = 1.27 \times 10^{-2}$ [m], and $g_7 = 4.63 \times 10^{-3}$ [m]. Moreover, $\Omega_{FoV}$ has been defined by setting in (7) $\zeta_{TH} = 10$ % and choosing $\psi_{TH}$ so that the maximum array scan loss is $-6$ [dB] (i.e., $\psi_{TH} = -6 + \psi_1(90, 0)$ [dB]). As for the array synthesis method, the requirement that no magnitude tapering is allowed (i.e., $\left|w^+_{nq}\right| = 1$, $n = 1, \ldots, N$ and $q = 1, \ldots, Q$), so that only the phases of the excitations are optimized (*PO*), has been encoded into the feasibility set $\mathcal{W}$ and the criterion for selecting the optimal trade-off array

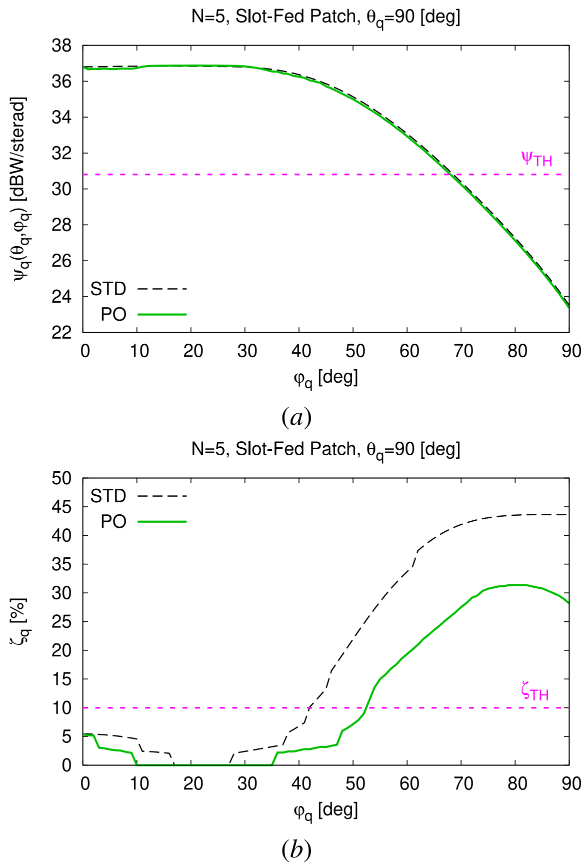


**FIGURE 5.** ***Slot-fed patch linear array* ($N = 5$, $f = 2$ [GHz], $d = 0.47\lambda$, $\theta_q = 90$ [deg]) - Plots of (a) $\psi_q(\theta_q, \varphi_q)$ and (*b*) $\zeta_q$ versus $\varphi_q$ ($q = 1, \dots, Q$; $Q = 91$).**

(i.e., $\underline{\underline{W}}^{+}\Big\rfloor_{opt}$) has been defined by setting $\Phi_{RAD}^{PO} \equiv \Phi_{RAD}^{STD}$, $\Phi_{RAD}^{STD}$ being (11) of the standard approach (*STD*) where the excitation phases are computed with the analytic linear phase shifting rule [17]. Finally, the $\varepsilon$-*MOEA* optimizer has been configured according to reference guidelines [22], [23], [24] by choosing the following setup: $\{\varepsilon_1, \varepsilon_2\} = \{5 \times 10^{-3}, 2.5 \times 10^{-2}\}$, $P = 50$, and $C = 1000$.

To illustrate the features and the behavior of the proposed method for a generic $q$-th ($q = 1, \dots, Q$) scan angle, Fig. 2($c$) shows the Pareto front $\mathcal{A}_{Cq}$ when $(\theta_q, \varphi_q) = (90, 52)$ [deg] ($\rightarrow q = 53$). As it can be observed the *PO* Pareto front [1] dominates the *STD* solution and the optimal trade-off array [i.e., the "green" cross in Fig. 2($c$)] reduces the total reflected power percentage from $\zeta_q^{STD} = 24.6$ % (i.e., $\Phi_{REFL}^{STD} = 0.246$) down to $\zeta_q^{PO} = 8.9$ % (i.e., $\Phi_{REFL}^{PO} = 0.089$), while keeping the same radiation performance (i.e., $\psi_q^{PO}(\theta_q, \varphi_q)\Big\rfloor_{q=53} = \psi_q^{STD}(\theta_q, \varphi_q)\Big\rfloor_{q=53} = 34.6$ [dBW/sterad] $\rightarrow$ $\Phi_{RAD} = 3.43 \times 10^{-4}$). The optimized excitations, which are reported in Fig. 3($a$), are very similar, which implies an analogous architectural complexity, while the corresponding *ARL* values are mitigated with respect to the *STD* approach [$ARL_{nq}^{PO} < ARL_{nq}^{STD}$, $n = 1, \dots, N$ - Fig. 3($b$)]. This latter outcome confirms that it is possible to indirectly control the *ARL* of a finite array by minimizing the total reflected power without reducing the radiated power along the steering direction (i.e., dashed magenta line in Fig. 4), although slightly modifying the sidelobe profile and

[1]The overall Pareto front $\mathcal{A}_{Cq}$ shows that, for a given array physical architecture, better radiation performance corresponds to worse *ARL* and vice versa (i.e., a low total reflected power does not correspond to a high power density in the target steering direction, in general, even though it may yield to an increased total radiated power).

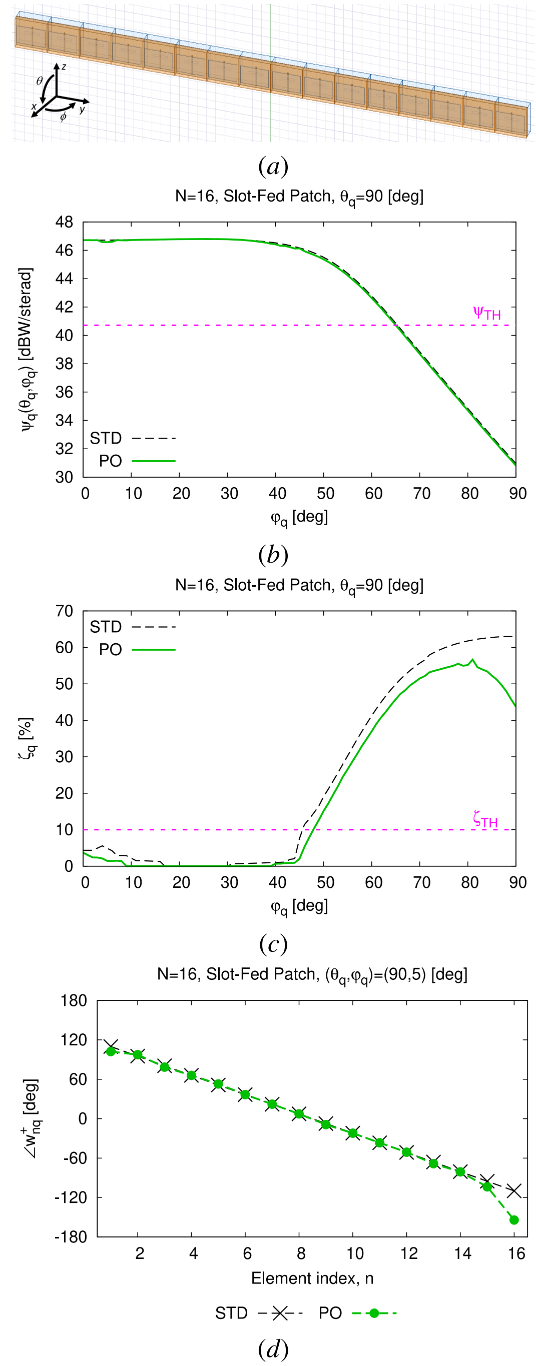


**FIGURE 6.** ***Slot-fed patch linear array* ($N = 16$, $f = 2$ [GHz], $d = 0.47\lambda$, $\theta_q = 90$ [deg]) - Sketch of (a) the HFSS model of the array, plots of (*b*) $\psi_q(\theta_q, \varphi_q)$, and (*c*) $\zeta_q$ versus $\varphi_q$ ($q = 1, \dots, Q$; $Q = 91$), and (*d*) behaviour of $\angle w_{nq}^{+}$ when $q = 6$, $(\theta_q, \varphi_q) = (90, 5)$ [deg].**

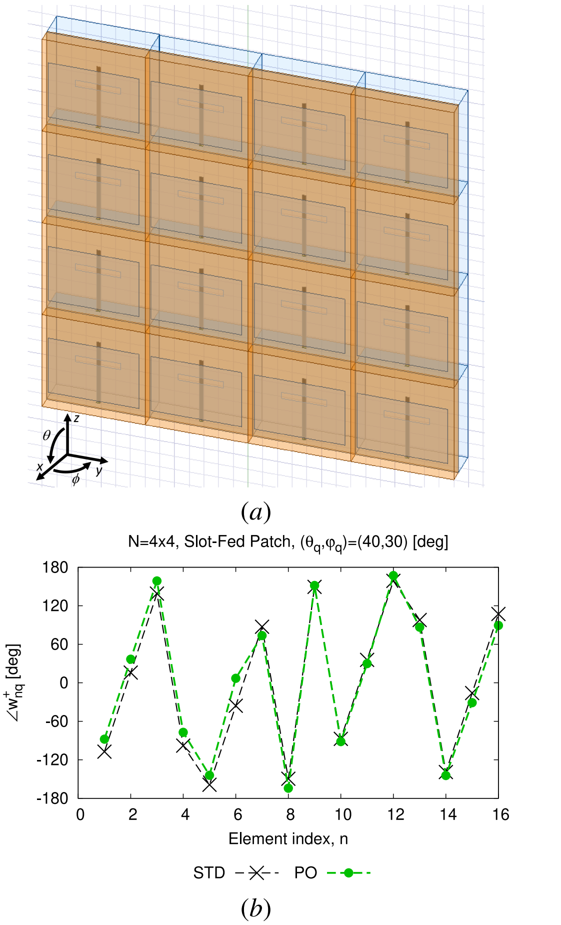


**FIGURE 7.** ***Slot-fed patch planar array*** **($N = 4 \times 4$, $f = 2$ [GHz], $d_x = d_y = 0.47\lambda$) - Sketch of the HFSS model of the array (a) and behaviour of $\angle w_{nq}^{+}$ when $q = 211$, $(\theta_q, \varphi_q) = (40, 30)$ [deg] (*b*).**

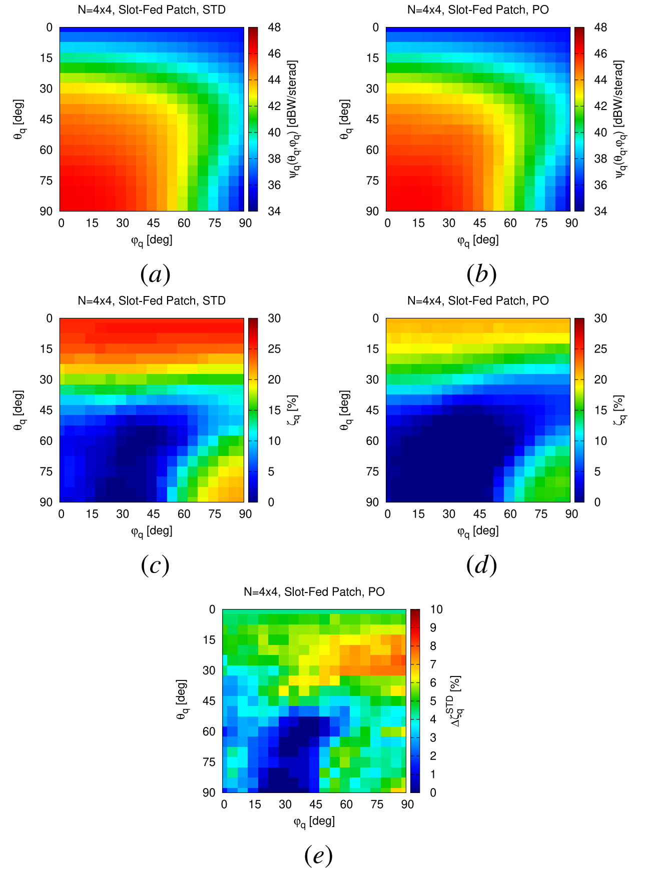


**FIGURE 8.** ***Slot-fed patch planar array*** **($N = 4 \times 4$, $f = 2$ [GHz], $d_x = d_y = 0.47\lambda$) - Plots of (a)(b) $\psi_q(\theta_q, \varphi_q)$, (c)(d) $\zeta_q$, and (e) $\Delta\zeta_q^{STD}$ ($q = 1, \dots, Q$; $Q = 361$).**

main beam peak location (Fig. 4). As for the computation time and resources for optimizing such a layout, less than 3 minutes were required exploiting a non-optimized MATLAB implementation of the method running on a single-core 1.60 GHz CPU-laptop using less than 100 MByte of RAM. Moreover, it is worth remarking that such resources scale linearly with the array size, hence turning out efficient even for large arrangements.

The resume of the *PO* performance for the first test case is given in Fig. 5 where the plots of the radiated power density, $\psi_q(\theta_q, \varphi_q)$ ($q = 1, \dots, Q$; $Q = 91$) [Fig. 5(*a*)], and the total reflected power percentage, $\zeta_q$ ($q = 1, \dots, Q$; $Q = 91$) [Fig. 5(*b*)], are reported. The scan width of the finite array is enlarged of about 22 [deg] (i.e., $-42$ [deg] $\leq \Omega_{FoV}^{STD} \leq 42$ [deg] vs. $-53$ [deg] $\leq \Omega_{FoV}^{PO} \leq 53$ [deg]), which corresponds to an increment of the field of view percentage $\alpha_{FoV}$ ($\alpha_{FoV} \triangleq \frac{Q_{FoV}}{Q}$) from $\alpha_{FoV}^{STD} \approx 46$ % up to $\alpha_{FoV}^{PO} \approx 58$ % ($\rightarrow \Delta\alpha_{FoV} \approx 12$ %) and a maximum reduction of the reflected power within $\Omega_{FoV}^{PO}$ that amounts to $\Delta\zeta_{max}^{STD} = 15.7$ % [$\Delta\zeta_{max}^{STD} \triangleq \max_{q=1,\dots,Q_{FoV}}\left(\Delta\zeta_q^{STD}\right)$ being $\Delta\zeta_q^{STD} \triangleq \zeta_q^{STD} - \zeta_q^{PO}$].

The applicability of the considered approach to wider linear arrays is assessed next by considering a larger arrangement with $N = 16$ elements [Fig. 6(*a*)]. While there is still a widening of the *FoV* [Figs. 6(*b*)-6(*c*)], the improvement with respect to the *STD* layout is here smaller ($\Delta\alpha_{FoV} \approx 4$ % $\rightarrow \Delta\Omega_{FoV} \approx 8$ [deg]) since the efficiency of the proposed method in balancing the input power among the array elements is vanified by the uniform coupling among the majority of them. This result suggests that (*i*) the margin of improvement enabled by the proposed method is influenced by the number and arrangement of the antenna elements, and that (*ii*) the mutual interactions in larger arrangements mitigate the achievable advantages. The plots of the optimized excitations of a representative $N = 16$ element solution (i.e., $q = 6$, $(\theta_q, \varphi_q) = (90, 5)$ [deg]) is provided in Fig. 6(*d*). for completeness.

The third test case is concerned with planar architectures. Towards this end, a planar $N = 4 \times 4$ arrangement of radiators as in Fig. 2(*a*) has been considered [Fig. 7(a) - $d_x = d_y = 0.47\,\lambda$] and the results from the *STD* and the *PO* syntheses are summarized in Fig. 8 by showing the color maps of $\psi_q(\theta_q, \varphi_q)$ ($q = 1, \dots, Q$; $Q = 361$) [Figs. 8(*a*)-8(*b*)] and $\zeta_q$ ($q = 1, \dots, Q$; $Q = 361$) [Figs. 8(*c*)-8(*d*)], together with the optimized excitations of a representative solution [i.e., $q = 211$, $(\theta_q, \varphi_q) = (40, 30)$ [deg] - Fig. 7(*b*)]. As expected, Figs. 8(*a*)-8(*b*) are almost identical by definition since the

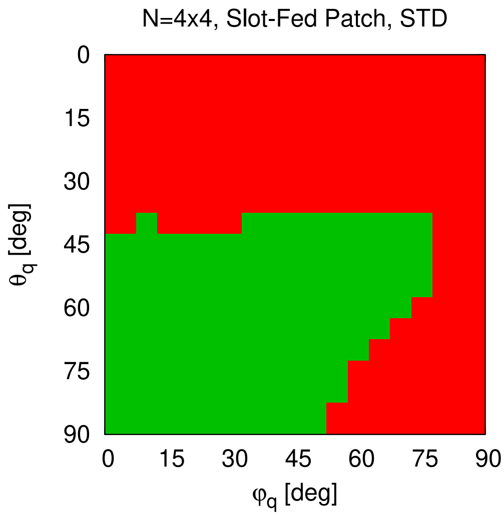


(*a*)

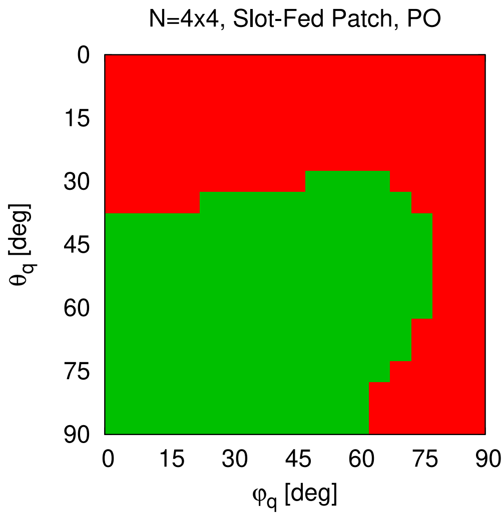


(*b*)

**FIGURE 9.** ***Slot-fed patch planar array*** **($N = 4 \times 4$, $f = 2$ [GHz], $d_x = d_y = 0.47\lambda$) - Plot of $\Omega^{FoV}$ (in green) of (a) the *STD* and (*b*) the *PO* arrays.**

criterion for selecting the "optimal" trade-off solution forces the condition $\Phi_{RAD}^{PO} \approx \Phi_{RAD}^{STD}$. Otherwise, the advantage of the *PO* approach is evident when comparing Fig. 8($c$) and Fig. 8($d$) and it is further highlighted in Fig. 8(e) where the reduction of the total reflected power, $\Delta\zeta_q^{STD}$ ($q = 1, \dots, Q$; $Q = 361$) is reported, $\Delta\zeta_{max}$ being equal to $\Delta\zeta_{max} \approx 8$ %. Therefore, the main outcome (i.e., the scanning performance of the finite array) is that the *PO* widens the field of view percentage from $\alpha_{FoV}^{STD} \approx 40$ % [Fig. 9($a$)] up to $\alpha_{FoV}^{PO} \approx 49$ % [Fig. 9($b$)] ($\rightarrow$ $\Delta\alpha_{FoV} \approx 9$ %).

The final numerical experiment is aimed at further assessing the *PO*-based solutions also against recently introduced wide scan layouts [28].[2]

[2]Reference [28] has been selected for the comparisons because it demonstrates excellent wide-scan performance and it provides detailed information concerning the array architecture and the optimized excitation coefficients.

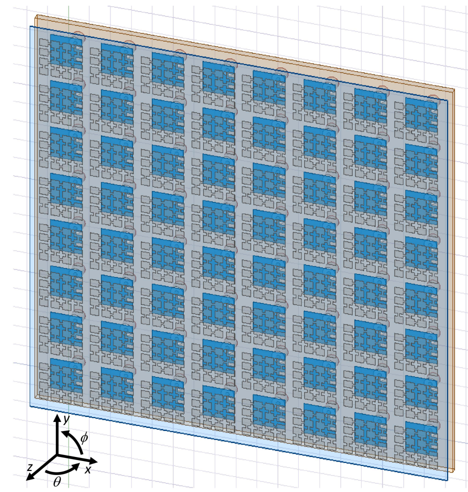


(*a*)

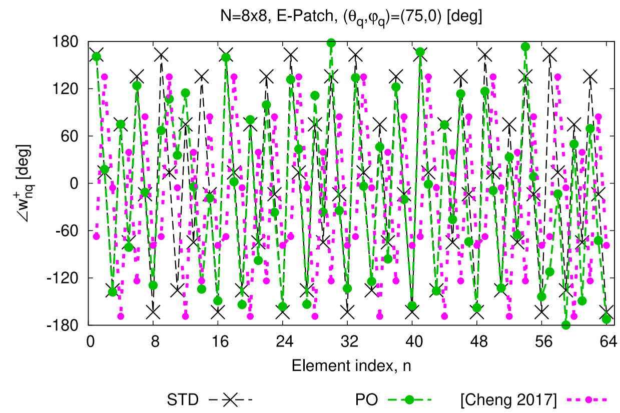


(*b*)

**FIGURE 10.** ***Pin-fed E-patch planar array*** **($N = 8 \times 8$, $f = 5.2$ [GHz], $d_x = 0.42\lambda$, $d_y = 0.43\lambda$) - Sketch of the HFSS model of the array (a) and behaviour of $\angle w_{nq}^{+}$ when $q = 34$, $(\theta_q, \varphi_q) = (75, 0)$ [deg] (*b*).**

Accordingly, a planar arrangement of $N = 8 \times 8$ ($d_x = 0.42\lambda$, $d_y = 0.43\lambda$) identical parasitic pixel layer-based E-shaped radiators [28] operating at $f = 5.2$GHz has been numerically modeled in Ansys HFSS [Fig. 10($a$)].

For comparison purposes, the plots of both the radiated power density and the total reflected power along the cut $\varphi_q = 0$ [deg] are shown in Fig. 11 where the values in Table 1 [28] are reported, as well, along with $\angle w_{nq}^{+}$ of representative solutions [i.e., $q = 34$, $(\theta_q, \varphi_q) = (75, 0)$ [deg] - Fig. 10($b$)]. Once again the *PO* array outperforms the *STD* one yielding on the $\varphi_q = 0$ [deg] plane an improvement of the *FoV* of about $\Delta\alpha_{FoV} \approx 13.2$ % ($\alpha_{FoV}^{STD} \approx 35.4$ % vs. $\alpha_{FoV}^{PO} \approx 48.6$ % [Figs. 11($a$)-11($b$)]), while it turns out to be $\Delta\alpha_{FoV} \approx 22.6$ % in the whole angular range [Fig. 12($a$) vs. Fig. 12($b$)].

The *PO* layout is also better than that in [28] in terms of $\psi_q(\theta_q, 0)$ and $\zeta_q$ ($q = 1, \dots, Q$; $Q = 37$) at the available angular samples (i.e., $\theta_4 = -75$ [deg], $\theta_8 = -55$ [deg], $\theta_{30} = 55$ [deg], and $\theta_{34} = 75$ [deg]) since 2.49 [dB] $\leq$ $\Delta\psi_q^{[Cheng\,2017]}(\theta_q, 0)$ $\leq$

**TABLE 1.** ***Pin-fed E-patch planar array* ($N = 8 \times 8$, $f = 5.2$ [GHz], $d_x = 0.42\lambda$, $d_y = 0.43\lambda$, $\varphi_q = 0$ [deg]) - Performance indexes.**

| $q$ | $(\theta_q, \varphi_q)$ | $\psi_q^{PO}(\theta_q, \varphi_q)$ | $\psi_q^{[Cheng\ 2017]}(\theta_q, \varphi_q)$ | $\psi_q^{STD}(\theta_q, \varphi_q)$ | $\zeta_q^{PO}$ | $\zeta_q^{[Cheng\ 2017]}$ | $\zeta_q^{STD}$ |
|---|---|---|---|---|---|---|---|
| 4 | $(-75, 0)$ | **41.83** | 35.97 | 41.40 | **2.98** | 27.62 | 28.30 |
| 8 | $(-55, 0)$ | **41.32** | 22.79 | 41.45 | **13.42** | 23.35 | 24.30 |
| 30 | $(55, 0)$ | **46.91** | 44.42 | 47.02 | **14.80** | 23.35 | 23.16 |
| 34 | $(75, 0)$ | **46.76** | 40.83 | 46.91 | **17.28** | 27.43 | 26.68 |

**TABLE 2.** ***Pin-fed E-patch planar array* ($N = 8 \times 8$, $f = 5.2$ [GHz], $d_x = 0.42\lambda$, $d_y = 0.43\lambda$, $\varphi_q = 0$ [deg]) - Performance indexes in [28].**

| $q$ | $(\theta_q, \varphi_q)$ | $SLL_q^{PO}$ | $SLL_q^{[Cheng\ 2017]}$ | $SLL_q^{STD}$ | $G_q^{PO}$ | $G_q^{[Cheng\ 2017]}$ | $G_q^{STD}$ | $\Delta\Theta_q^{PO}$ | $\Delta\Theta_q^{[Cheng\ 2017]}$ | $\Delta\Theta_q^{STD}$ |
|---|---|---|---|---|---|---|---|---|---|---|
| 4 | $(-75, 0)$ | **−2.12** | −5.78 | −5.38 | **6.57** | 6.56 | 7.38 | **3.55** | 4.03 | 3.75 |
| 8 | $(-55, 0)$ | **−3.82** | −5.68 | −5.44 | **6.54** | 6.04 | 7.04 | **3.71** | 1.86 | 2.26 |
| 30 | $(55, 0)$ | **−8.83** | −10.06 | −9.85 | **12.16** | 11.78 | 12.47 | **2.77** | 2.17 | 2.22 |
| 34 | $(75, 0)$ | **−9.06** | −9.29 | −9.61 | **12.22** | 11.79 | 12.62 | **5.06** | 0.94 | 4.94 |

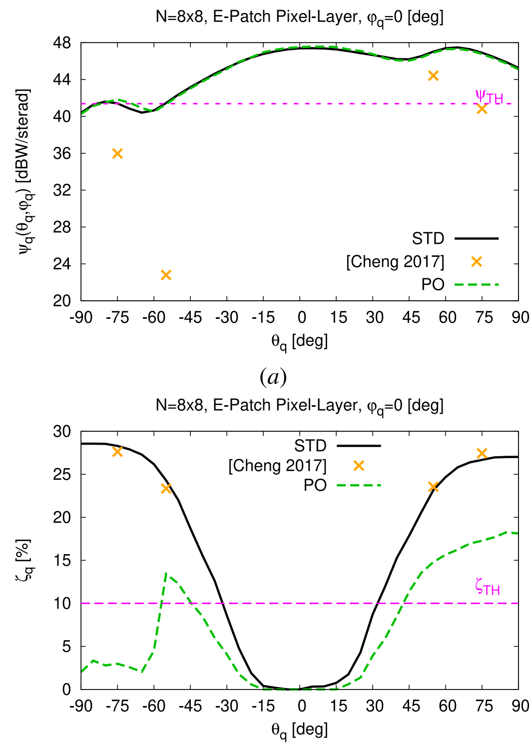


**FIGURE 11.** ***Pin-fed E-patch planar array* ($N = 8 \times 8$, $f = 5.2$ [GHz], $d_x = 0.42\lambda$, $d_y = 0.43\lambda$, $\varphi_q = 0$ [deg]) - Plots of (a) $\psi_q(\theta_q, \varphi_q)$ and (b) $\zeta_q$ versus $\theta_q$ ($q = 1, \ldots, Q$; $Q = 37$).**

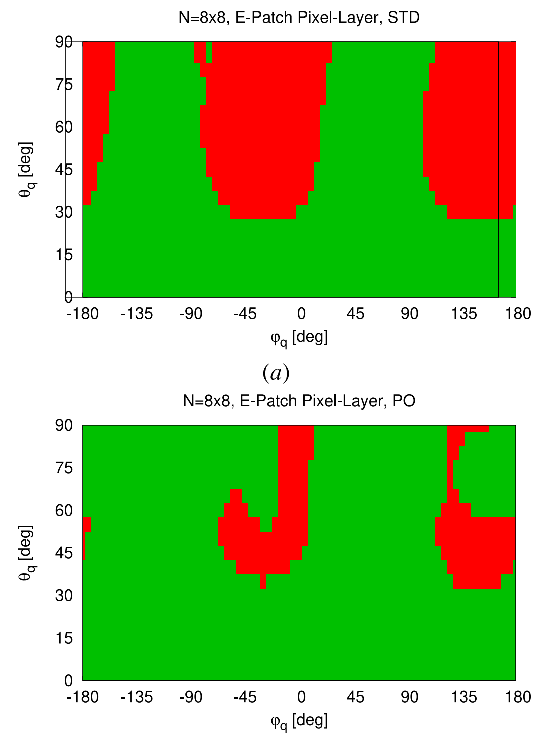


**FIGURE 12.** ***Pin-fed E-patch planar array* ($N = 8 \times 8$, $f = 5.2$ [GHz], $d_x = 0.42\lambda$, $d_y = 0.43\lambda$) - Plot of $\Omega^{FoV}$ (in green) of (a) the *STD* and (*b*) the *PO* arrays.**

18.35 [dB] ($\Delta\psi_q^{[Cheng\ 2017]}(\theta_q, \varphi_q) \triangleq \psi_q^{PO}(\theta_q, \varphi_q) - \psi_q^{[Cheng\ 2017]}(\theta_q, \varphi_q)$ [dB]) and 8.8 % $\leq \Delta\zeta_q^{[Cheng\ 2017]} \leq$ 24.64 % in Table 1. For fairness, the comparison has been also carried out by considering the figures-of-merit optimized in [28] and the outcomes are summarized in Table 2 where $SLL_q$, $G_q$, and $\Delta\Theta_q$ are the normalized sidelobe level ($SLL_q \triangleq \frac{\max_{(\theta,\varphi)\notin ML} \psi_q(\theta,\varphi)}{\max_{(\theta,\varphi)} \psi_q(\theta,\varphi)}$, $ML$ being the main-lobe region), the array gain ($G_q \triangleq 4\pi \frac{\max_{(\theta,\varphi)} \psi_q(\theta,\varphi)}{\mathbb{P}_q^{IN}}$), and the scan angle error ($\Delta\Theta_q \triangleq \theta_q - \arg\{\max_{(\theta,\varphi)} \psi_q(\theta, \varphi)\}$), respectively. As it can be noticed (Table 2), the values for the two layouts are quite similar (i.e., $-3.66$ [dB] $\leq \Delta SLL_q^{[Cheng\ 2017]} \leq$ $-0.23$ [dB], 0.01 [dB] $\leq \Delta G_q^{[Cheng\ 2017]} \leq$ 0.50 [dB], and $-0.48$ [deg] $\leq \Delta\Theta_q^{[Cheng\ 2017]} \leq$ 4.12 [deg]). These results remark that, owing to the nature of the design problem, the proposed trade-off solution exhibit improved performance in terms of radiated power density and total reflected power with respect to the technique in [28] (bold values in Table 1), while yielding sub-optimal, although very close, sidelobe and scan angle performance (e.g., bold values in Table 2).

Finally, Fig. 13 gives the color level maps of the *ARL* of the $N = 8 \times 8$ array elements when $(\theta_q, \varphi_q) = (-75, 0)$ [deg] (i.e., $q = 4$), $ARL_{nq}$ ($n = 1, \ldots, N$), for the *PO* [Fig. 13(*a*)], the *SoA* [28] [Fig. 13(*b*)], and the *STD* [Fig. 13(*c*)] layouts. As it can be observed, generally

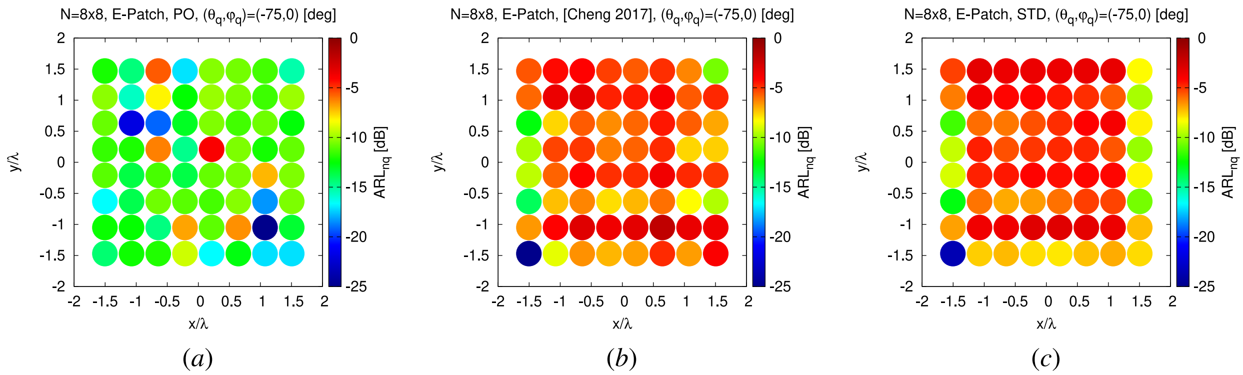


**FIGURE 13.** ***Pin-fed E-patch planar array*** **($N = 8 \times 8$, $f = 5.2$ [GHz], $d_x = 0.42\lambda$, $d_y = 0.43\lambda$, $q = 4$, $(\theta_q, \varphi_q) = (-75, 0)$ [deg]) - Plots of $ARL_{nq}$, $n = 1, \ldots, N$ of (*a*) *PO*, (*b*) *SoA* [28], and (*c*) the *STD* arrays.**

$ARL_{nq}^{PO} < ARL_{TH}$ $(n = 1, \ldots, N;\ q = 4)$, $ARL_{TH} = -10$ [dB]. This outcome further assesses the capability of the *PO*-based synthesis to indirectly control the *ARL* of a finite array by minimizing the total reflected power without reducing the radiated power along the steering direction. Moreover, the condition $ARL_{nq}^{PO} < ARL_{nq}^{[Cheng\,2017]}$ $(q = 4)$ holds true in several $n$-th $(n = 1, \ldots, N)$ radiating elements [Fig. 13(*a*) vs. Fig. 13(*b*)], while $ARL_{nq}^{[Cheng\,2017]} \approx ARL_{nq}^{STD}$ $(n = 1, \ldots, N;\ q = 4)$.

## IV. CONCLUSION AND OBSERVATIONS

The synthesis of the excitations of antenna arrays to achieve wide-angle scanning features (i.e., a wide *FoV*) with minimum reflected power has been addressed. Towards this end, an innovative methodology has been proposed by formulating the array synthesis as a multi-objective problem where, for each scan angle, both the radiated power density in the scan direction and the total reflected power are accounted for by including the finite array coupling in the design process (i.e., no periodicity approximation is employed). The effectiveness of the approach has been assessed with a selected set of numerical test cases by also proving the possibility to indirectly control the *ARL* of finite arrays.

The main outcomes from the numerical validation, which has been carried out with a commercial and industry-standard full-wave software [27] to have a faithful modelling of all the electromagnetic interactions and distortions caused by non-idealities, can be summarized as follows:

- the implemented design concept outperforms the standard linear phase shifting technique [17] in yielding wide-angle scanning arrays regardless of the frequency, the radiating elements, and the array arrangement (i.e., linear or planar);
- the *PO*-based synthesis method allows one to enhance the *FoV* of finite antenna arrays without modifying the antenna architecture, thus it can be applied to upgrade existing arrays;
- the multi-objective design process provides the user with a multiplicity of trade-off Pareto-front solutions, thus the possibility of choosing an optimal one depending on an application-driven criterion based on either functional or non-functional (e.g., costs, maintenance, etc$\cdots$) constraints;
- the proposed scheme has non-negligible advantages over recent alternative approaches such as [28].

Future works, beyond the scope of this manuscript, will be aimed at extending the proposed methodology to conformal structures. Moreover, the realization and subsequent measurement of a reconfigurable phased array prototype for the validation of the presented results, currently impossible in our University owing to the lack of suitable resources and facilities, will be addressed in future contributions at least on a small-scale case to verify the accuracy of the simulation results and the practical feasibility of the proposed method.

## ACKNOWLEDGMENT

A. Massa wishes to thank E. Vico for her never-ending inspiration, support, guidance, and help.

## REFERENCES

[1] J. S. Herd and M. D. Conway, “The evolution to modern phased array architectures,” *Proc. IEEE*, vol. 104, no. 3, pp. 519–529, Mar. 2016.
[2] S. Gao, Y. J. Guo, S. A. Safavi-Naeini, W. Hong, and X.-X. Yang, “Guest editorial: Low-cost wide-angle beam-scanning antennas,” *IEEE Trans. Antennas Propag.*, vol. 70, no. 9, pp. 7378–7383, Sep. 2022.
[3] G. Oliveri et al., “Wide-angle impedance matching layer-enhanced dual-polarization sub-6 GHz wide-scan array for next-generation base stations,” *IEEE Trans. Antennas Propag.*, vol. 70, no. 7, pp. 5506–5520, Jul. 2022.
[4] R. C. Hansen, *Phased Array Antennas*. Hoboken, NJ, USA: Wiley, Inc., 2009.
[5] S. E. Valavan, D. Tran, A. G. Yarovoy, and A. G. Roederer, “Dual-band wide-angle scanning planar phased array in X/Ku-bands,” *IEEE Trans. Antennas Propag.*, vol. 62, no. 5, pp. 2514–2521, May 2014.
[6] S. E. Valavan, D. Tran, A. G. Yarovoy, and A. G. Roederer, “Planar dual-band wide-scan phased array in X-band,” *IEEE Trans. Antennas Propag.*, vol. 62, no. 10, pp. 5370–5375, Oct. 2014.
[7] C.-M. Liu, S. Xiao, and X.-L. Zhang, “A compact, low-profile wire antenna applied to wide-angle scanning phased array,” *IEEE Antennas Wireless Propag. Lett.*, vol. 17, no. 3, pp. 389–392, Mar. 2018.
[8] R. Xia, S. Qu, X. Bai, Q. Jiang, S. Yang, and Z. Nie, “Experimental investigation of wide-angle impedance matching of phased array using overlapped feeding network,” *IEEE Antennas Wireless Propag. Lett.*, vol. 13, pp. 1284–1287, 2014.
[9] R.-L. Xia, S.-W. Qu, P.-F. Li, D.-Q. Yang, S. Yang, and Z.-P. Nie, “Wide-angle scanning phased array using an efficient decoupling network,” *IEEE Trans. Antennas Propag.*, vol. 63, no. 11, pp. 5161–5165, Nov. 2015.

[10] S. Sajuyigbe, M. Ross, P. Geren, S. A. Cummer, M. H. Tanielian, and D. R. Smith, "Wide angle impedance matching metamaterials for waveguide-fed phased-array antennas," *Inst. Eng. Technol. Microw. Antennas Propag.*, vol. 4, no. 8, pp. 1063–1072, Aug. 2010.
[11] G. Oliveri, F. Viani, N. Anselmi, and A. Massa, "Synthesis of multilayer WAIM coatings for planar-phased arrays within the system-by-design framework," *IEEE Trans. Antennas Propag.*, vol. 63, no. 6, pp. 2482–2496, Jun. 2015.
[12] G. Oliveri, M. Salucci, N. Anselmi, and A. Massa, "Multiscale system-by-design synthesis of printed WAIMs for waveguide array enhancement," *IEEE J. Multiscale Multiphys. Comput. Techn.*, vol. 2, pp. 84–96, 2017.
[13] G. Oliveri, A. Polo, M. Salucci, G. Gottardi, and A. Massa, "SbD-based synthesis of low-profile *WAIM* superstrates for printed patch arrays," *IEEE Trans. Antennas Propag.*, vol. 69, no. 7, pp. 3849–3862, Jul. 2021.
[14] P. Hannan, D. Lerner, and G. Knittel, "Impedance matching a phased-array antenna over wide scan angles by connecting circuits," *IEEE Trans. Antennas Propag.*, vol. 13, no. 1, pp. 28–34, Jan. 1965.
[15] E. G. Magill and H. A. Wheeler, "Wide-angle impedance matching of a planar array antenna by a dielectric sheet," *IEEE Trans. Antennas Propag.*, vol. AP-14, no. 1, pp. 49–53, Jan. 1966.
[16] D. M. Pozar, "The active element pattern," *IEEE Trans. Antennas Propag.*, vol. 42, no. 8, pp. 1176–1178, Aug. 1994.
[17] R. J. Mailloux, *Phased Array Antenna Handbook*, 2nd Ed. Norwood, MA, USA: Artech House, 2005.
[18] G. Oliveri, G. Gottardi, and A. Massa, "A new meta-paradigm for the synthesis of antenna arrays for future wireless communications," *IEEE Trans. Antennas Propag.*, vol. 67, no. 6, pp. 3774–3788, Jun. 2019.
[19] G. Oliveri, G. Gottardi, N. Anselmi, and A. Massa, "Capacity-driven low-interference fast beam synthesis for next generation base stations," *IEEE Trans. Antennas Propag.*, vol. 70, no. 6, pp. 4472–4484, Jun. 2022.
[20] D. M. Pozar, "A relation between the active input impedance and the active element pattern of a phased array," *IEEE Trans. Antennas Propag.*, vol. 51, no. 9, pp. 2486–2489, Sep. 2003.
[21] C. A. Balanis, *Advanced Engineering Electromagnetics*, New York, NY, USA: Wiley, 1989.
[22] K. Deb, M. Mohan, and S. Mishra, "A fast multi-objective evolutionary algorithm for finding well-spread Pareto-optimal solutions," KanGAL, Kanpur, India, Rep. 2003002, Feb. 2003.
[23] M. Laumanns, L. Thiele, K. Deb, and E. Zitzler, "Combining convergence and diversity in evolutionary multiobjective optimization," *Evol. Comput.*, vol. 10, no. 3, pp. 263–282, Sep. 2002.
[24] P. Rosatti, M. Salucci, L. Poli, and A. Massa, "Multiobjective system-by-Design for mm-Wave automotive radar antennas," *IEEE Trans. Antennas Propag.*, vol. 71, no. 4, pp. 2958–2973, Apr. 2023.
[25] P. Rocca, M. Benedetti, M. Donelli, D. Franceschini, and A. Massa, "Evolutionary optimization as applied to inverse scattering problems," *Invers Probl.*, vol. 25, no. 12, pp. 1–41, Dec. 2009.
[26] W.Y. Chiu, G. G. Yen, and T. K. Juan, "Minimum Manhattan distance approach to multiple criteria decision making in multiobjective optimization problems," *IEEE Trans. Evol. Comput.*, vol. 20, no. 6, pp. 972–985, Dec. 2016.
[27] *ANSYS Electromagnetics Suite-HFSS*, ANSYS, Inc., Canonsburg, PA, USA, 2021.
[28] Y.-F. Cheng, X. Ding, W. Shao, M.-X. Yu, and B.-Z. Wang, "2-D Planar wide-angle scanning-phased array based on wide-beam elements," *IEEE Antennas Wireless Propag. Lett.*, vol. 16, pp. 876–879, 2017.

**PIETRO ROSATTI** (Student Member, IEEE) received the B.Sc. degree in electronics and telecommunications engineering, the M.Sc. degree in information and communication engineering, and the Ph.D. degree in information engineering and computer science from the University of Trento, Italy, in 2017, 2020, and 2024, respectively. He is currently a Postdoctoral Fellow with the University of Trento and a Researcher with the ELEDIA Research Center. His research activity is focused on the design and analysis of wide angle phased array antennas for modern applications as automotive radars and 5G communications.

**GIACOMO OLIVERI** (Fellow, IEEE) received the B.S. and M.S. degrees in telecommunications engineering and the Ph.D. degree in space sciences and engineering from the University of Genoa, Italy, in 2003, 2005, and 2009 respectively. He is currently an Associate Professor with the Department of Civil, Environmental, and Mechanical Engineering, University of Trento, and a Board Member of the ELEDIA Research Center. Moreover, he is an Adjunct Professor with CentraleSupélec and a member of the Laboratoire des signaux et systèmes (L2S), CentraleSupélec, Gif-sur-Yvette, France. He has been a Visiting Researcher with L2S in 2012, 2013, and 2015, an Invited Associate Professor with the University of Paris Sud, France, in 2014, and a Visiting Professor with Université Paris-Saclay in 2016 and 2017. He is the author/co-author of over 400 peer reviewed papers on international journals and conferences. His research work is mainly focused on electromagnetic direct and inverse problems, multifunctional metamaterials engineering, and antenna array synthesis. He served as an Associate Editor for the IEEE ANTENNAS AND WIRELESS PROPAGATION LETTERS from 2016 to 2022 and for the IEEE JOURNAL ON MULTISCALE AND MULTIPHYSICS COMPUTATIONAL TECHNIQUES from 2017 to 2023. He is an AE of *EPJ Applied Metamaterials*, of the *International Journal of Antennas and Propagation*, of the *International Journal of Distributed Sensor Networks*, of the *Microwave Processing*, and of the *Sensors*. He is the Chair of the IEEE AP/ED/MTT North Italy Chapter. He has been serving as the Chair of the AP-S IEEE Press Liaison Committee, as a member of the IEEE AP-S Field Award Subcommittee, and as a member of the IEEE AP-S Membership and Benefit Committee. He has been elected as an IEEE AP-S AdCom Member for the triennium from 2025 to 2027.

**ANDREA MASSA** (Fellow, IEEE) has been a Full Professor of Electromagnetic Fields with the University of Trento since 2005. He is currently the Director of the Network of Federated Laboratories "ELEDIA Research Center" located in Brunei, China, Czech, Ethiopia, France, Greece, Italy, Japan, Perù, and Tunisia, with more than 150 researchers. Moreover, he is a Holder of a Chang-Jiang Chair Professorship with UESTC, Chengdu, China, a Visiting Research Professor with the University of Illinois at Chicago, Chicago, USA, a Distinguished Visiting Professor with Tsinghua, Beijing, China, a Visiting Professor and an IAS Distinguished Scholar with Tel Aviv University, Tel Aviv, Israel, and a Professor with CentraleSupélec, Paris, France. He has been a Holder of a Senior DIGITEO Chair with L2S-CentraleSupélec and CEA LIST in Saclay, France, a UC3M-Santander Chair of Excellence with the Universidad Carlos III de Madrid, Spain, an Adjunct Professor with Penn State University, USA, a Guest Professor with UESTC, and a Visiting Professor with the Missouri University of Science and Technology, USA, the Nagasaki University, Japan, the University of Paris Sud, France, the Kumamoto University, Japan, and the National University of Singapore, Singapore. He published more than 900 scientific publications among which more than 350 on international journals (>17.000 citations - h-index = 69 [Scopus]; > 14.000 citations - H-index = 63 [ISI-WoS]; > 28.000 citations - H-index = 95 [Google Scholar]) and more than 570 in international conferences, where he presented more than 210 invited contributions (> 50 invited keynote speaker). He has organized more than 100 scientific sessions in international conferences and has participated to several technological projects in the national and international framework with both national agencies and companies (18 international prj, > 5 M€; 8 national prj, > 5 M€; 10 local prj, > 2 M€; 63 industrial prj, > 10 M€; and 6 university prj, > 300 K€). His research activities are mainly concerned with inverse problems, antenna analysis/synthesis, radar systems and signal processing, cross-layer optimization and planning of wireless/RF systems, system-by-design and material-by-design (meta-materials and reconfigurable-materials), and theory/applications of optimization techniques to engineering problems (coms, medicine, and biology). He has been appointed as an IEEE AP-S Distinguished Lecturer from 2016 to 2018 and served as an Associate Editor for the IEEE TRANSACTION ON ANTENNAS AND PROPAGATION from 2011 to 2014. He is an IET Fellow and an Electromagnetic Academy Fellow.